Modelling and Control Solution of an E-axle for Third-Generation Electric Vehicles

Modelling and Control Solution of a E-axle for Third-Generation Electric Vehicles

Andres Sierra-Gonzalez[1], Paolo Pescetto[2], Elena Trancho[1], Gianmario Pellegrino[2]

[1]Tecnalia, Basque Research and Technology Alliance (BRTA), 48160 Derio, Spain

[2]Politecnico Di Torino, 10129 Torino, Italy

Abstract This work studies the use of an e-axle based on a six-phase IPMSM. In addition, it has a dc bus with a cascade configuration. Moreover, a dc/dc converter is incorporated between the battery module and the six-phase inverter to provide the vehicle with fast charging capabilities, while avoiding the use of power semiconductors with high nominal voltages. In this scenario, the control algorithm must cope with the non-linearities of the machine by providing an accurate setpoint command for the entire torque and speed range of the inverter. Therefore, cross-coupling effects between the windings must be considered, and the voltage of the cascade link capacitors must be actively controlled and balanced. Given this, the authors propose a novel control approach that provides all these functionalities. The proposal has been experimentally validated on a full-scale prototype 70 kW electric drive, tested in a laboratory and an electric vehicle under real driving conditions.

Introduction

The transition to a circular economy and the profound decarbonization of our economies and lifestyles has never been more urgent. In December 2019, the EU authorized the European Green Deal Action Plan in response to these challenges. This plan aims to transform the Union into a modern, resource-efficient, competitive, and inclusive economy by 2050, decoupling economic growth from resource consumption and attaining carbon neutrality across all economic sectors. In this context, the decarbonization of transportation is crucial. To achieve carbon neutrality by 2050, this sector, which accounts for roughly one-fourth of the Union's greenhouse gas emissions, must undergo a tremendous transition to electrification.
In this scenario, The EU-funded FITGEN project aimed to develop a functionally integrated e-axle (motor-inverter-transmission) ready for implementation in third-generation electric vehicles. The FITGEN e-axle is delivered at TRL-7 by the end

of the project, and it is demonstrated on the FIAT 500e electric vehicle platform. The FITGEN e-axle aimed to increase the power density of the e-motor by 40 % and the power density of the inverter by 50 % compared to the best-in-class market-available technology at the project start. The daily electric driving range of the demonstrator is required to go from 740 to 1,050 km with three battery recharges, by using the e-axle in-built super-fast charging capability.

To meet the FITGEN project's goals, the e-axle depicted in Fig. 1 was designed and developed. This e-axle is equipped with a high-speed symmetrical six-phase IPMSM. The machine development takes advantage of a patented design with three layers of permanent magnets and flux barriers [1] and state-of-the-art patented Formed Litz wire winding technology [2]. Thanks to this, the machine prototype achieved a gravimetric power density of 5.3 kW/kg, stand-alone efficiency of 97.4%, low torque ripple, low back electro-motive force voltage, and a high reluctance torque. The electrical machine is driven by a six-phase inverter, with a switching frequency of up to 24 kHz. This inverter was designed using wide bandgap SiC power metal-oxide-semiconductor field-effect transistors. Thanks to the SiC technology's higher efficiency, smaller size and better thermal performance, the inverter prototype exhibits a volumetric power density of 35 kW/l.

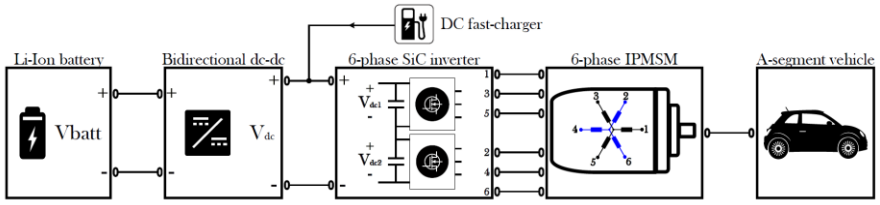

Fig. 1 General diagram of the FITGEN e-axle including a dc/dc converter, a six-phase SiC-based inverter with a cascaded dc-link capacitor, and a dual three-phase IPMSM.

In addition, a bidirectional dc/dc converter is affixed between the battery pack and power inverter on the e-axle. This converter increases the dc-link voltage to the 800 V range, enabling ultra-fast charging compatibility. Furthermore, the 800V dc-link allows high dynamic performance of the IPMSM at high speed. Nevertheless, a cascaded dc-link configuration has been adopted to avoid the use of power semiconductors with high voltage ratings, which have greater conduction losses and are more expensive. This configuration consists of two series-connected three-phase inverter units, with each unit driving one of the machine windings sets [3]. Furthermore, the high-speed machine is coupled to a single-gear high-speed transmission. Such a gearbox was designed to operate at its top speed of more than 20,000 rpm while maintaining great efficiency. Reduced weight and cost were achieved due to the lack of a pump and corresponding control system thanks to a passive lubrication/cooling system.

This work presents the design and validation results of the control solution proposed for FITGEN's e-axle. First, the dynamic models used for the design of the controller are presented. Then, the design of the control solution is described, and the experimental validation results are shown. Finally, the conclusions are presented.

Dynamic model of the multiphase electrical machine

Control systems rely on accurate representations of the electrical machine dynamics to provide stable and precise control of motor torque. Furthermore, dynamic models allow a fast and low-cost assessment of the performance of the e-axle in different operating scenarios and load conditions. By simulating the system behaviour, parameters like response time, efficiency, power consumption, and transient behaviour can be analyzed. This section describes the modelling approaches that can be used for six-phase machines. First, the mathematical equations modelling the dynamics in the natural per-phase variables are developed. Then, two vector model approaches, *multiphase* and *double three-phase*, are described.

For a 6-phase machine, the stator voltage equation in the natural variable reference frame is:

$$\boldsymbol{V} = \boldsymbol{RI} + \frac{d\boldsymbol{L}}{dt}\boldsymbol{I} + \boldsymbol{L}\frac{d\boldsymbol{I}}{dt} + \frac{d\Psi_{\boldsymbol{PM}}}{dt}, \quad \textbf{(1)}$$

where $\mathbf{V} = [\boldsymbol{v_1}, \boldsymbol{v_2}, \boldsymbol{v_3}, \boldsymbol{v_4}, \boldsymbol{v_5}, \boldsymbol{v_6}]^{\boldsymbol{T}}$ and $\mathbf{I} = [\boldsymbol{i_1}, \boldsymbol{i_2}, \boldsymbol{i_3}, \boldsymbol{i_4}, \boldsymbol{i_5}, \boldsymbol{i_6}]^{\boldsymbol{T}}$ are the per-phase voltages and currents, respectively. $\mathbf{R}$ is a $\boldsymbol{6} \times \boldsymbol{6}$ diagonal matrix, where each diagonal element represents the phase resistance. On the other hand, $\boldsymbol{L}$ is the $\boldsymbol{6} \times \boldsymbol{6}$ stator inductance matrix. Each element $\boldsymbol{L_{ij}}(\boldsymbol{i}, \boldsymbol{j} \in \{\boldsymbol{1}, \boldsymbol{2}, \dots, \boldsymbol{6}\})$ represents the self $(\boldsymbol{i} = \boldsymbol{j})$ and mutual inductances $(\boldsymbol{i} \neq \boldsymbol{j})$ between phases *i* and *j*. Considering the spatial distribution of the windings, $\boldsymbol{L}$ is a symmetric matrix. The term $\boldsymbol{\Psi_{PM}}$ is the 6-dimensional flux linkage vector ($\boldsymbol{\Psi_{PM}} = [\boldsymbol{\psi_1}, \boldsymbol{\psi_2}, \dots, \boldsymbol{\psi_6}]$) generated due to the permanent magnets For IPMSMs, the elements of $\boldsymbol{L}$ and $\boldsymbol{\Psi_{PM}}$ vary according to the rotor electrical angle ($\boldsymbol{\theta_e}$). This is produced because of the variable magnetic reluctance of such rotor configuration [4]. Moreover, $\boldsymbol{L}$ and $\boldsymbol{\Psi_{PM}}$ varies with the stator currents due to magnetic saturation.

The next step is to model the electromagnetic torque produced by the machine. This model can be derived from the conventional electrical input power equation ($P = I^{TV}$). First, the non-torque-producing terms are removed (copper and magnetic losses). Finally, the expression that relates output power and torque is used ($P = \omega_{mec} T_{em}$) to get the electromagnetic torque equation:

$$\boldsymbol{T_{em}} = \frac{\boldsymbol{1}}{\boldsymbol{2}}\boldsymbol{I}^{\boldsymbol{T}}\frac{\boldsymbol{dL}}{\boldsymbol{d\theta_m}}\boldsymbol{I} + \boldsymbol{I}^{\boldsymbol{T}}\frac{\boldsymbol{\Psi_{PM}}}{\boldsymbol{d\theta_m}}, \quad \textbf{(2)}$$

Thus, (2) completes the mathematical representation of the electric machine. However, such a model is complex and highly coupled, not suitable for control system design. Therefore, vector transformations are applied to simplify the mathematical representation of the model by decoupling and eliminating dependence on rotor position. These transformations allow the design and implementation of the well-known FOC technique [5].

The first vector transformation T_1 is obtained by multiplying the decoupling transformation matrix C_1 in (3) and the rotating transformation matrix P_1 in (4), i.e., $T_1 = P_1 C_1$.

$$C_1 = \frac{1}{3}\begin{bmatrix} 1 & cos(\alpha) & cos(2\alpha) & cos(3\alpha) & cos(4\alpha) & cos(5\alpha) \\ 0 & sin(\alpha) & sin(2\alpha) & sin(3\alpha) & sin(4\alpha) & sin(5\alpha) \\ 1 & cos(2\alpha) & cos(4\alpha) & cos(6\alpha) & cos(8\alpha) & cos(10\alpha) \\ 0 & sin(2\alpha) & sin(4\alpha) & sin(6\alpha) & sin(8\alpha) & sin(10\alpha) \\ 1 & 0 & 1 & 0 & 1 & 0 \\ 0 & 1 & 0 & 1 & 0 & 1 \end{bmatrix} \quad (3)$$

$$P_1 = \begin{bmatrix} cos(\theta_e) & sin(\theta_e) & 0 & 0 & 0 & 0 \\ -sin(\theta_e) & cos(\theta_e) & 0 & 0 & 0 & 0 \\ 0 & 0 & cos(5\theta_e) & sin(5\theta_e) & 0 & 0 \\ 0 & 0 & -sin(5\theta_e) & cos(5\theta_e) & 0 & 0 \\ 0 & 0 & 0 & 0 & 1 & 0 \\ 0 & 0 & 0 & 0 & 0 & 1 \end{bmatrix} \quad (4)$$

Where $\alpha = \pi/3$, is the spatial separation between adjacent phases in symmetrical six-phase machines. Applying $\boldsymbol{T_1}$ to (1) and (2), the *multiphase* vector model is obtained:

$$v_{D1} = R_s i_{D1} + L_{D1}\frac{di_{D1}}{dt} - \omega_e L_{Q1} i_{Q1}$$
$$v_{Q1} = R_s i_{Q1} + L_{Q1}\frac{di_{Q1}}{dt} + \omega_e (L_{D1} i_{D1} + \psi_{PM1}) \quad (5)$$

$$v_{D2} = R_s i_{D2} + L_{D2}\frac{di_{D2}}{dt} - 5\omega_e L_{Q2} i_{Q2}$$
$$v_{D2} = R_s i_{D2} + L_{D2}\frac{di_{D2}}{dt} - 5\omega_e L_{Q2} i_{Q2} \quad (6)$$

$$T_{em} = 3N_p\left[\psi_{PM1} i_{Q1} + \left(L_{D1} - L_{Q1}\right) i_{D1} i_{Q1}\right] \quad (7)$$

This vector model shows that both planes $D_1 - Q_1$ and $D_2 - Q_2$ are decoupled, where the frame $D_1 - Q_1$ contains the fundamental components, while the subspace $D_2 - Q_2$ comprises the 5th and 7th harmonics [5]. From (7), it is deduced that torque can be controlled by only regulating the $D_1 - Q_1$ plane currents. Therefore, the optimal current references are easier to calculate, with the advantage that cross-coupling between the two three-phase sets is considered.

The second vector transformation $\boldsymbol{T_2}$ is obtained by multiplying matrices C_2 and P_2.

$$C_2 = \frac{2}{3}\begin{bmatrix} 1 & cos(2\alpha) & cos(4\alpha) & 0 & 0 & 0 \\ 0 & sin(2\alpha) & sin(4\alpha) & 0 & 0 & 0 \\ 0.5 & 0.5 & 0.5 & 0 & 0 & 0 \\ 0 & 0 & 0 & 1 & cos(2\alpha) & cos(4\alpha) \\ 0 & 0 & 0 & 0 & sin(2\alpha) & sin(4\alpha) \\ 0 & 0 & 0 & 0.5 & 0.5 & 0.5 \end{bmatrix} \quad (8)$$

$$P_2 = \begin{bmatrix} cos(\theta_e) & sin(\theta_e) & 0 & 0 & 0 & 0 \\ -sin(\theta_e) & cos(\theta_e) & 0 & 0 & 0 & 0 \\ 0 & 0 & 1 & 0 & 0 & 0 \\ 0 & 0 & 0 & cos(\theta_e - \alpha) & sin(\theta_e - \alpha) & 0 \\ 0 & 0 & 0 & -sin(\theta_e - \alpha) & cos(\theta_e - \alpha) & 0 \\ 0 & 0 & 0 & 0 & 0 & 1 \end{bmatrix} \quad (9)$$

As previously, applying $\boldsymbol{T_2}$ to (1) and (2), the *double three-phase* vector model is obtained:

$$\begin{aligned} v_{d1} &= R_s i_{d1} + L_d \frac{di_{d1}}{dt} - \omega_e L_q i_{q1} + M_d \frac{di_{d2}}{dt} - \omega_e M_q i_{q2} \\ v_{q1} &= R_s i_{q1} + L_q \frac{di_{q1}}{dt} + \omega_e L_d i_{d1} + M_q \frac{di_{q2}}{dt} + \omega_e M_d i_{d2} + \omega_e \psi_{PM} \end{aligned} \quad \textbf{(10)}$$

$$\begin{aligned} v_{d2} &= R_s i_{d2} + L_d \frac{di_{d2}}{dt} - \omega_e L_q i_{q2} + M_d \frac{di_{d1}}{dt} - \omega_e M_q i_{q1} \\ v_{q2} &= R_s i_{q2} + L_q \frac{di_{q2}}{dt} + \omega_e L_d i_{d2} + M_q \frac{di_{q1}}{dt} + \omega_e M_d i_{d1} + \omega_e \psi_{PM} \end{aligned} \quad \textbf{(11)}$$

$$\begin{aligned} T_{em} = \frac{3}{2} N_p \big[\psi_{PM} \{(i\}_{q1} + i_{q2}) + (L_d - L_q)(i_{d1} i_{q1} + i_{d2} i_{q2}) \\ + (M_d - M_q)(i_{d1} i_{q2} + i_{d2} i_{q1}) \big] \end{aligned} \quad \textbf{(12)}$$

In this model, the $d_1 - q_1$ and $d_2 - q_2$ planes are coupled by the terms M_d and M_q. Therefore, the equations of voltages, currents, and torque are more complex than those of a three-phase machine. Another feature of applying T_2 is that both planes rotate at the same speed, but there is a $\pi/3$ offset between them. Both planes can produce torque, as shown by (12). The proposed control solution benefits from both vector models.

Design and validation of the control solution

Fig. 2 shows the block diagram of the control solution designed for the e-axle [6], which can be viewed in three stages. The first stage considers the required torque, dc-link and stator voltages, and rotor speed to calculate the optimal electric current setpoints. These are computed by LUTs, compiled using a high-fidelity mathematical model in the *D*-*Q* synchronous frame to simplify the representation of the complex non-linear and coupled behaviour of the IPMSM. To reduce the LUTS's required dimensions and increase the controller's robustness against system parameter variation, a VCT loop is incorporated. To achieve this, the VCT varies the speed fed to the LUTs and keeps the stator voltages in a safe range.

The second stage comprises the dc voltage active balancing algorithm, necessitated by the cascaded topology of the 6-phase SiC-inverter, which balances the input voltages of the sub-inverters. To do so, first, the current references are transformed ($\boldsymbol{T_{1\to 2}}$) to the *d*-*q* synchronous frame to facilitate the independent regulation of each three-phase set. Then, a PI controller modifies the current setpoints to balance the DC voltage of each three-phase set. Note that only *q*-axis setpoints are modified to avoid disturbing the operation at high speeds or field weakening. As required in an automotive application, the algorithm operates correctly in motoring and regenerative braking.

The third stage contains synchronous current regulation via PI-FOC featuring feed-forward decoupling and anti-windup schemes. Additionally, carrier-based Pulse-Width Modulation blocks synthesize the firing pulses for each sub-inverter.

In addition to regulating torque, the system optimizes e-axle efficiency by adopting a variable dc-link strategy to dynamically adapt the inverter bus voltage based on the e-motor operating point. The dc-link variation is enabled by the high-performance dc/dc converter located between the battery and the 6-phase inverter. A custom control strategy minimizes the dc-link voltage without affecting control dynamics and minimizes switching losses in the drive and the dc/dc converter [7].

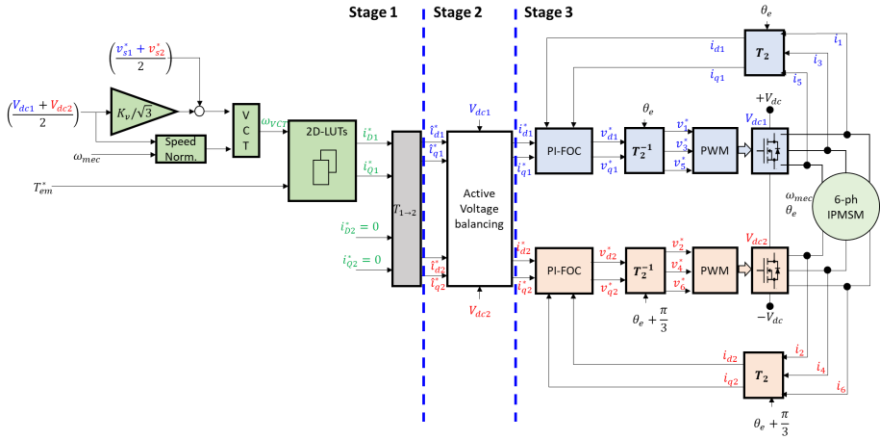

Fig. 2 General block diagram of the proposed control solution

The proposed control solution was experimentally validated. First, the control system is validated at TRL-6 over a laboratory test bench, incorporating a full-scale prototype with a peak power of 135~kW, developed within the context of the FITGEN project. These initial tests show the need of implementing an interleaved PWM modulation scheme due to the presence of overlapping windings in the machine's stator. After this modification, the controller is extensively tested in the laboratory under various operation profiles, including several driving cycles. Next, the drive prototype is integrated into a real EV, and the novel controller is validated at TRL-7, both in dynamometer and on-road tests. For example, Fig. 3 shows the experimental results obtained under the US06 driving cycle. The right-side charts present a stretch of the US06 cycle at maximum speed, demonstrating accurate torque tracking during sharp torque commands, proper voltage balancing, and regulation of the stator voltages below the maximum admissible value.

Conclusions

The control approach conveniently combines two vector representations to meet automotive requirements such as torque control accuracy, safe operation, and low

computational burden. This approach successfully addressed the highly coupled and non-linear nature of the six-phase e-axle with cascaded configuration. Thanks to the TRL-7 validation, the industrial applicability of dual three-phase IPMSM drives with cascaded dc-link configuration is assessed, and the proposed control solution is fully validated for their utilization in real automotive applications.

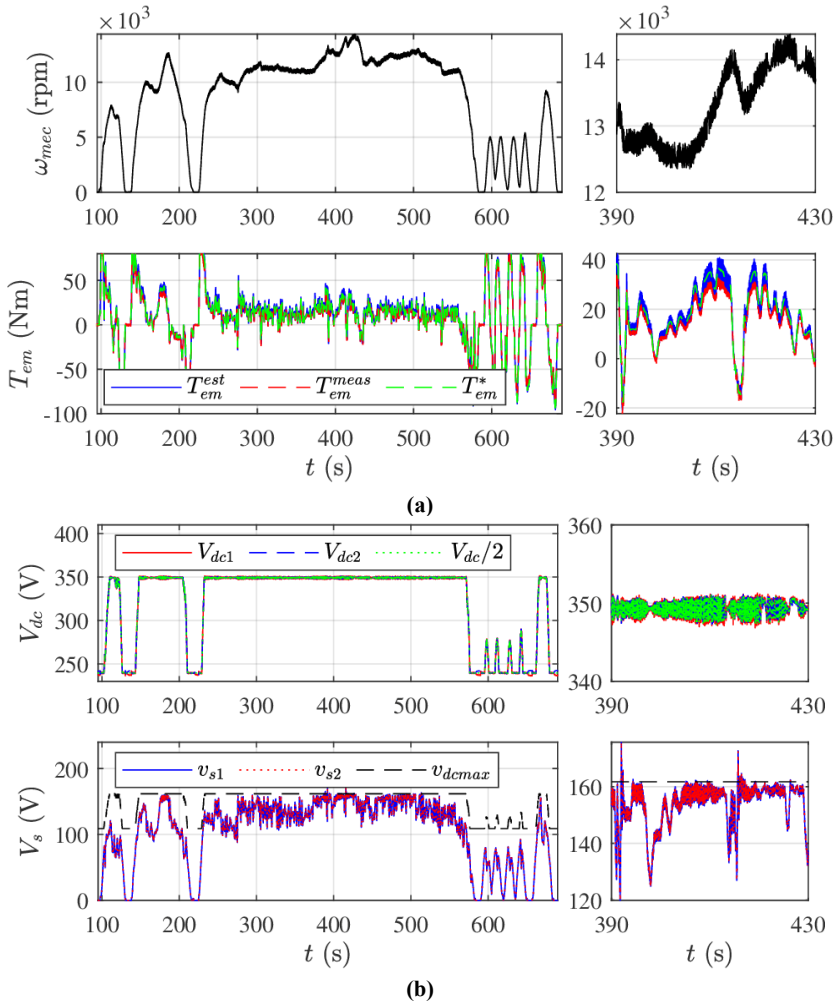

Fig. 3 Experimental results obtained under the US06 driving cycle.

References

[1] Zhou T., Oeschger D., Teufel R., Muntean A. (2018): Rotor for a synchronous drive motor. EU Patent EP3651316A1, 2018
[2] Dimier T., Cossale M., Wellerdieck T. (2020): Comparison of Stator Winding Technologies for High-Speed Motors in Electric Propulsion Systems, In: International Conference on Electrical Machines (ICEM) Gothenburg (2020), 10.1109/ICEM49940.2020.9270943
[3] Martino M., Pescetto P., Pellegrino G. (2020): Advanced Functionally Integrated E-Axle for A-Segment Electric Vehicles, In: AEIT International Conference of Electrical and Electronic Technologies for Automotive Turin (2020), 10.23919/AEITAUTOMOTIVE50086.2020.9307382
[4] Rahman M. (2016): Power Electronics and Motor Drives, CRC Press, 2016, Ch. Permanent Magnet Machines, ISBN 9781138077478
[5] Karttunen J., Kallio S., Peltoniemi P., Silventoinen P., and Phyronen O. (2014): Decoupled vector control scheme for dual three-phase permanent magnet synchronous machines, IEEE Transactions on Industrial Electronics, Volume 61, 2014, ISSN 1557-9948
[6] Sierra-Gonzalez A., Pescetto P., Alvarez-Gonzalez F., Heriz B., Trancho E., Lacher H., Ibarra E., Pellegrino G. (2023): Full-Speed Range Control of a Symmetrical Six-Phase Automotive IPMSM Drive with a Cascaded DC-link Configuration, IEEE Transactions on Industry Applications, Volume 59, 2023, ISSN 1939-9367
[7] Pescetto P., Sierra-Gonzalez A., Alvarez-Gonzalez F., Kapeller H., Trancho E., Lacher H., Pellegrino G. (2023): Active Control of Variable DC-Link for Maximum Efficiency of Traction Motor Drives, IEEE Transactions on Industry Applications, Early Access, 2023, ISSN 1939-9367

List of abbreviations

IPMSM	Interior Permanent Magnet Synchronous Machine
LUT	Loop Up Table
PI-FOC	Proportional Integral Field Oriented Controller
SiC	Silicon-Carbide
VCT	Voltage Control Tracking

Acknowledgement

This chapter was based on work conducted in the EU H2020 project FITGEN, (Grant agreement 824335).